Investigation of Turbulent Transport in an Axisymmetric Sudden Expansion

Richard D. Gould*
North Carolina State University, Raleigh, North Carolina
and
Warren H. Stevenson† and H. Doyle Thompson‡
Purdue University, West Lafayette, Indiana

Simultaneous two-component laser velocimeter measurements were made in the incompressible turbulent flowfield following an axisymmetric sudden expansion. Mean velocities, Reynolds stresses, and triple products were measured and are presented at axial positions ranging from $x/H = 0.2$–14. A balance of the turbulent kinetic energy in the flow was performed. The production, convection, and diffusion of turbulent kinetic energy were computed directly from the experimental data using central differencing. A specially designed correction lens was employed to correct for optical aberrations introduced by the circular tube. This lens system allowed the accurate simultaneous measurement of axial and radial velocities in the test section. The experimental measurements were compared to predictions generated by a code that employed the k-ϵ turbulence model. Agreement was good for mean axial velocities, turbulent kinetic energy, and turbulent shear stresses. However, the modeled turbulent normal stresses where in poor agreement with the measured values. The modeled diffusion of turbulent kinetic energy was underpredicted in the region between the shear layer and the centerline of the flow giving lower values of turbulent kinetic energy downstream of the potential core than measured.

Nomenclature

C_D = turbulence constant, = 0.09
H = step height, 38.1 mm
k = turbulent kinetic energy, $= (\overline{uu} + \overline{vv} + \overline{ww})/2$
l = mixing length, mm
P = time-averaged mean static pressure, N/m^2
p = pressure fluctuation about time-averaged mean, N/m^2
R_1 = inlet radius of sudden expansion, 38.1 mm
R_2 = outlet radius of sudden expansion, 76.2 mm
r = radial coordinate direction, (= 0 at centerline)
U = time-averaged mean axial velocity, m/s
U_0 = inlet reference velocity, 22 m/s
u = fluctuating axial velocity, m/s
$\overline{up}$ = time-averaged axial velocity-ressure correlation, N/m-s
$\overline{uu}$ = time-averaged axial turbulent normal stress, m^2/s^2
$\overline{uv}$ = time-averaged turbulent shear stress, m^2/s^2
$\overline{uuu}$ = turbulent triple product, m^3/s^3
$\overline{uuv}$ = turbulent triple product, m^3/s^3
$\overline{uvv}$ = turbulent triple product, m^3/s^3
V = time-averaged mean radial velocity (positive toward wall), m/s
v = fluctuating radial velocity, m/s
$\overline{vp}$ = time-averaged radial velocity-pressure correlation, N/m-s
$\overline{vv}$ = time-averaged radial turbulent normal stress, m^2/s^2
$\overline{vvv}$ = turbulent triple product, m^3/s^3
w = fluctuating tangential velocity, m/s
$\overline{ww}$ = time-averaged tangential turbulent normal stress, m^2/s^2
x = axial coordinate direction
y = radial coordinate direction, (= 0 at centerline)
ϵ = dissipation of turbulent kinetic energy, m^2/s^3
μ = dynamic viscosity, Kg/m-s
μ_t = turbulent viscosity, Kg/m-s
μ_{eff} = effective viscosity, Kg/m-s
ρ = fluid density, kg/m^3
σ = standard deviation

Introduction

THE flow downstream of a sudden pipe expansion is of both theoretical and practical importance since it involves a number of fundamental flow phenomena and is found in a wide variety of important applications. Due to the axial symmetry of the flow, experimental measurements can be compared directly with numerical models without the difficulties that arise in two-dimensional (2-D) rectangular cross sections as a result of sidewall boundary layer effects. Therefore, a complete and accurate experimental mapping of the flowfield would provide a significant data base for testing of various models. The present study was initiated with this in mind.

Flowfield properties of interest include axial and radial mean velocities and turbulent normal stresses as well as Reynolds stresses. Triple products are also measured. A two-color, two-component laser velocimeter was used to make these measurements. Aberrations introduced by the circular tube were compensated for by a specially designed correction lens system developed by Durrett et al.[1] Special attention was given to the velocity bias issue, since bias error can be significant in regions of high turbulence which are of most interest.

Background

The separated flow following a sudden expansion is complex, consisting of a potential core, a curved free-shear layer with high turbulence levels, a primary recirculation zone, and a secondary recirculation zone or corner eddy very close to the step. Following reattachment of the shear layer at the wall, the flow proceeds to develop and in the case of an axisymmetric

Received Jan. 23, 1989; revision received May 15, 1989.

*Assistant Professor, Mechanical and Aerospace Engineering Department.
†Professor, School of Mechanical Engineering.
‡Professor, School of Mechanical Engineering. Associate Fellow AIAA.

sudden expansion, a fully developed turbulent pipe flow is achieved.

Numerous studies of 2-D and axisymmetric sudden expansions have been conducted. Comprehensive reviews of 2-D step-flow studies have been presented by Eaton and Johnston[2] and Bremmer et al.[3] Driver and Seegmiller[4] presented a rather complete data set of two-component laser Doppler velocimeter (LDV) measurements in a 2-D step flow and compared them with state-of-the-art turbulence modeling predictions. Pitz and Daily[5] investigated the reacting flowfield following a 2-D step. Stevenson et al.[6] reviewed a number of axisymmetric sudden expansion flow investigations including those of Freeman[7] and Moon and Rudinger,[8] which were the first in which LDV measurements were reported. Freeman's work was conducted with water, whereas Moon and Rudinger used air as the working medium. Gould et al.[9] investigated both air flow and flow with combustion in a sudden expansion. In all of the above axisymmetric sudden expansion studies, a single-component LDV system was used and measurements were confined to the tube diameter coinciding with the optical axis of the LDV system. Radial velocity measurements in an axisymmetric geometry were first performed by Durrett et al.[10] by using a specially designed correction lens system to compensate for aberrations introduced by the circular tube wall. Velocity measurements in the secondary recirculation zone were also made in the latter study.

Experimental Apparatus

LDV System

A two-color, two-component LDV system operating in forward scatter was developed to make simultaneous measurements of axial and radial velocity components in the axisymmetric sudden expansion flow. The LDV system included Bragg cell modulators in the four beam paths to allow a net frequency shift of 5 MHz in both the green and blue beams. This permitted an unambiguous measurement of negative velocities and also eliminated incomplete signal bias. Probe volume diameters of the green and blue beams were 250 μm and 150 μm, respectively. The probe volume lengths were approximately 2 mm, and the fringe spacings were 5.33 μm for the green probe volume and 5.11 μm for the blue probe volume. Scattered light from the probe volume was separated with a dichroic filter so that approximately 80% of each color passed to its respective photomultiplier tube. Narrow bandpass filters were used to reduce signal cross talk further.

The data collection and processing system consisted of two TSI Model 1990 countertype processors (one for each channel), a TSI Model 1998 interface with coincidence timing electronics, and a PDP 11/40 minicomputer with direct memory access capability. With this system, it was theoretically possible to acquire velocity data from individual Doppler burst signals at rates up to 10,000 samples/s. (In practice the rates were less due to seed density limits.) The minicomputer and counter processors were also interfaced so that sampling could be controlled. This was accomplished with a hardware clock controlling the data ready-inhibit handshaking signals.

Flow System

The flow system used for this experiment is illustrated in Fig. 1. It consisted of a converging inlet nozzle with an exit diameter of 76.2 mm followed by a 152.4-mm-diameter downstream section. This inlet was chosen to give a uniform inlet velocity profile. The test section was extruded from optical quality fused quartz and allowed measurements throughout the flowfield for x/H values ranging from 0.2–14. The test section design is shown in Fig. 2.

Air flow was provided by a radial fan blower followed by a flow conditioning section consisting of honeycomb flow

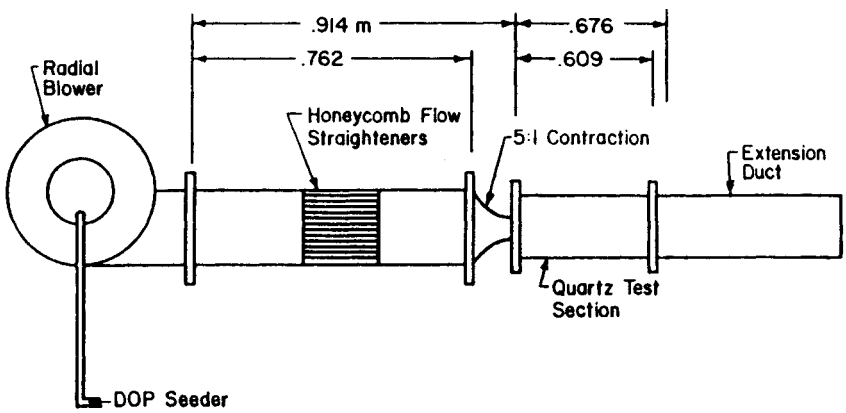

Fig. 1 Flow system

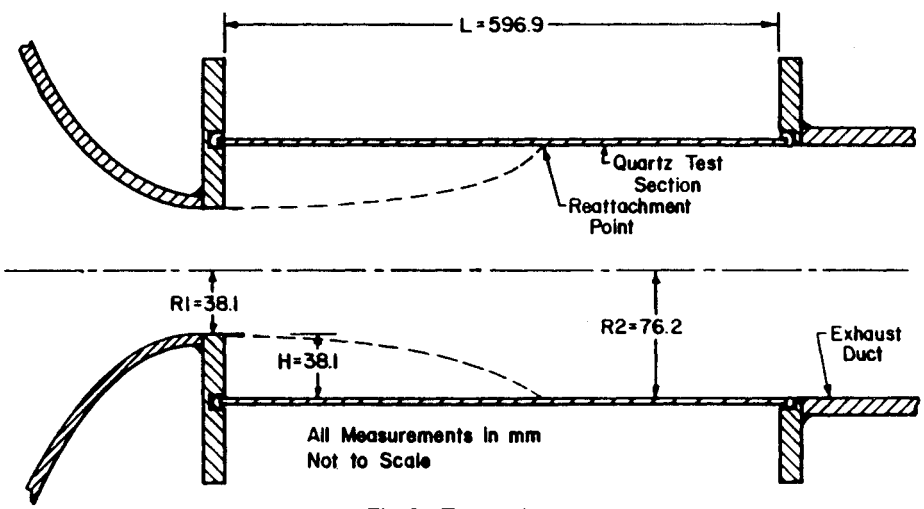

Fig. 2 Test section.

straighteners. The static pressure drop across the nozzle was used to monitor inlet flow conditions and was maintained constant to within ± 0.25 mm of water throughout the experiment.

Seeding was supplied by two TSI Model 3076 liquid atomizers each followed by TSI Model 3072 evaporation-condensation monodisperse aerosol generators. This produced seeding particles 1 μ or less in diameter using a 100% solution of dioctyl phthalate (DOP). The seeders were capable of providing seed densities sufficient to give data validation rates in excess of 30,000/s for each channel (green and blue beams) over most of the flowfield. The two-channel "coincident" data validation rate, which is controlled by the coincidence timing logic circuit in the TSI 1998 master interface, was somewhat less than the asynchronous data validation rates that the individual counter processors detect. With the coincidence window set to 10 μs, as it was for this experiment, the maximum "coincident" data validation rate was approximately one-half the value of the data rate reading on the counter processor with the lower of the two data rates. For this experiment, two-channel "coincident" data validation rates ranged between 10,000–15,000/s over most of the flowfield. This validation rate was high enough to permit eliminating velocity bias by inhibiting the counter processors for a fixed time interval between samples, approximating equal time sampling. This method has previously been described by Stevenson et al.[11] and its effectiveness confirmed in subsequent studies, including the work by Gould et al.,[9] Durrett et al.,[10] Johnson et al.,[12] and Gould et al.[13]

Correction Lens

A correction lens to allow simultaneous axial and radial velocity measurements in a cylindrical tube was designed using the procedure described by Durrett et al.[1] The planar-concave cylindrical lens that corrected for the aberration induced by the quartz test section had a radius of curvature of 3.3528 m, a thickness at its center of 17.93 mm, and a refractive index of 1.52. The correction lens insured that the orthogonal probe volumes (green and blue) intersected to within 100 μm along the length and to within 25 μm along the diameter. The system was comprised of two plano-concave cylindrical lenses, one on the transmitting side and one of the receiving side of the test section. Simultaneous axial-radial velocity measurements could be made to a nondimensional radius of approximately 83% with this sytem.

Experimental Technique

The simultaneous axial and radial velocities were sampled at 100 Hz using the interval sampling technique for velocity bias elimination discussed earlier. In all cases, 6400 individual realizations were accumulated for each velocity component at each measurement point to form velocity histograms. The relatively long sampling time (64 s) insured that all low-frequency phenomena were included in the sample. The Eulerian integral time scale was found to be on the order of 6 ms (150 Hz) in the shear layer of this flowfield.[13] Using statistical analysis and assuming Gaussian distributions (statistical independence) and local turbulence intensity levels of 70%, the expected sampling error for the 6400 sample size was found to be less than 1.8% for both mean and standard deviation values for a 95% confidence level.[14] All data points lying outside 3σ were discarded, and revised statistics were calculated. Typically, less than 50 data points out of the 6400 were discarded. This is higher than the theoretical number of discards for a 3σ cutoff (i.e., 20) because the accompanying sample was discarded if either one of the two simultaneous measurements was rejected.

Computational Flow Predictions

An existing TEACH computer program, originally developed by Pun and Spalding[15] and subsequently modified by Chiappetta,[16] for predicting the turbulent swirling and reacting flow in an axisymmetric bluff body combustor was further modified for this study. The modifications were limited to changing the boundary conditions to those for an axisymmetric sudden expansion. The code employs the two-equation k-ϵ turbulence model and the combustion model of Magnussen and Hjertager.[17] Since experimental measurements were made in nonswirling cold flow, conservation equations for swirl and chemical reaction were not solved for this study. The standard turbulence constants given by Pun and Spalding were used.

Inlet boundary conditions were extrapolated from the experimental data at $x/H = 0.2$. The axial inlet velocity was set to 22 m/s in the core region and a $\delta_{99\%} = 6.35$ mm boundary layer was patched from the edge of the core region to the wall. The radial inlet velocity was set to zero. The inlet turbulent kinetic energy was set to $k = 0.29\ \text{m}^2/\text{s}^2$ ($k/U_0^2 = 0.0006$) in the core region of the flow and increased to $k = 10\ \text{m}^2/\text{s}^2$ ($k/U_0^2 = 0.02$) in the boundary layer of the inlet in the fashion shown in Fig. 8. A mixing length l of 6.35 mm was chosen to define the inlet turbulent dissipation rate profile according to the definition $\epsilon = C_D^{0.75} k^{1.5}/l$. The mixing length value was based on the boundary-layer thickness obtained from the measured U and $\overline{uu}$ profiles at $x/H = 0.2$. This inlet boundary condition is the source of the greatest uncertainty in the calculations because a direct measurement of the mixing length was not made.

The outlet boundary conditions are that the axial gradients of the dependent variables vanish at the exit plane (fully developed flow). Care was taken to insure that the exit plane was far enough downstream so as to not influence the upstream results. Predictions were carried out with the exit plane located 20 step heights downstream of the inlet plane.

A bounded, skewed, upwind-differencing scheme developed by Raithby[18] was added to the TEACH code by Chiappetta.[16] The overall differencing method is a hybrid scheme that uses second-order central differencing when cell Reynolds numbers are less than 2 and uses skewed upwind differencing for cell Reynolds numbers of 2 or larger. This skewed differencing scheme uses a nine-point stencil and thereby accounts for the flow angle of the fluid into the control volume. Raithby has shown, for four simple test cases, that the errors generated using this hybrid scheme were approximately two orders of magnitude smaller than the errors generated using standard upwind differencing. The method reduces false diffusion effects that are inherent in standard upwind differencing.

Computations were made using both a 22×87 and a 42×87 grid in the radial and axial directions, respectively. The coarse grid results were virtually the same as the fine-grid-results for x/H values 5. However, differences in these two predictions did exist in the recirculation zone upstream of $x/H = 5$. For example, the turbulent kinetic energy profiles shifted and caused differences by as much as 25% at a few locations in the recirculation region. The results presented herein are from the fine-grid computation.

Validation of Modeled Turbulent Stresses

The TEACH code uses the k-ϵ turbulence model to predict the turbulent momentum transport. The steady-state solution of the TEACH code provides the values for the mean axial and radial velocities, U and V, the pressure P, the turbulent kinetic energy k, and the turbulent dissipation ϵ, at each node point in the flow domain. First-level validation of the code is made by directly comparing measured mean velocities with the predicted ones. The turbulent kinetic energy k, defined as

$$k = (\overline{uu} + \overline{vv} + \overline{ww})/2 \tag{1}$$

can also be compared directly with experimental measurements, giving a second level of validation. Experimental measurements of ϵ involve making two-point correlation measurements which are more difficult to obtain and therefore are not usually available for comparison. In this study, an additional level of code validation was performed to determine how well the k-ϵ turbulence model estimates the unknown turbulent normal stresses $\overline{u_i u_i}$ and the Reynolds stresses $\overline{u_i u_j}$. This vali-

dation is performed by reversing the modeling steps used in the k-ϵ turbulence closure procedure. The closure procedure is as follows. The turbulent viscosity μ_t in the k-ϵ model is given by

$$\mu_t = C_D \rho k^2/\epsilon \tag{2}$$

where C_D is an empirical coefficient and ρ is the density (assumed constant throughout the flow). Thus, in addition to the preceding five dependent variables, the value of μ_t is also known throughout the computational flow domain. The unknown turbulent normal and shear stresses are then found using μ_t and the mean velocity gradients through the modified Boussinesq approximation for constant density fluid[19]

$$-\rho\overline{u_i u_j} = \mu_t\left[\frac{\partial U_i}{\partial x_j} + \frac{\partial U_j}{\partial x_i}\right] - \frac{2}{3}\delta_{ij}[\rho k] \tag{3}$$

Now the unknown turbulent stresses in the time-averaged momentum equations are represented in terms of known parameters (U, V, k, and ϵ) and closure is obtained. The modification to the Boussinesq approximation is the inclusion of the last term which insures that the equation balances when the normal stresses ($i = j$) are summed. Calculating the modeled turbulent stresses that are used in the time-averaged momentum equations simply involves numerically differentiating the predicted mean axial and radial velocity distributions so that $\overline{u_i u_j}$ can be found using Eq. (3). These modeled turbulent stresses can now be compared directly with the measured values giving an even higher level of code validation. It should be noted that care must be taken when numerically differentiating the dependent variables due to the staggered grid used in TEACH codes.

Experimental Results and Discussion

Mean Velocity Data

LDV measurements of the axial and radial mean velocity and turbulent normal stresses as well as Reynolds stress, turbulent kinetic energy, and turbulent triple products were made in the axisymmetric sudden expansion flow and are presented here. The measurements were all direct and were made at 21 radial locations across the test section and at 12 axial planes located at nondimensional axial distances based on step height of $x/H = 0.2$–14. Figures 3–12 are profile plots of the normalized LDV measurements with comparisons of the numerically predicted values. Triple products are not used in the k-ϵ model, therefore no predicted values are shown in these plots. The mean inlet centerline velocity of 22 m/s was used to normalize all measurements. Figure 3 shows the measured mean axial velocity profiles throughout the sudden expansion flowfield. The inlet velocity profile was measured at $x/H = 0.2$ and found to be very flat across the entire diameter of the inlet. Velocity measurements on both sides of the centerline at this axial location indicated that the inlet profile was very symmetric. Results from previous studies,[6,9,10] including circumferential static pressure measurements, LDV measurements across the entire test section, and integrated mass flux balances at a number of axial planes, all indicated axial symmetry throughout the flowfield. Therefore, symmetry of the downstream flowfield was assumed, and LDV measurements were made along a radial line from the centerline of the flow out to 83% of the radius (limited by correction lens performance). Fairly good overall agreement exists between the measured and the computed values shown in Fig. 3, although the centerline velocity is first underpredicted and then overpredicted. This was also found in previous studies by Stevenson et al.[20] and Durrett et al.[10] The large discrepancy between the predicted and measured axial velocity near the centerline at $x/H > 10$ does not imply a mass balance error since the flow area for $r/R < 0.2$ accounts for only 4% of the total flow area. The model also predicts higher negative axial velocities in the recirculation zone than the experimental measurements indicate. Reattachment occurs at approximately 8 step heights downstream of the inlet plane, which agrees with published results from many earlier studies.

The mean radial velocity measurements show more data scatter than the axial velocity component, as can be seen in Fig. 4. This would be expected since the mean radial velocity is more than an order of magnitude smaller than the mean axial velocity over much of the flow. The error bar takes into account beam steering errors due to slight surface ripples on the extruded quartz tube wall and uncertainty in the orientation of the blue fringes with respect to the flow. Measured mean radial velocity is zero to within the uncertainty estimate across the diameter of the inlet and on the centerline at all downstream axial locations. The velocity profiles presented here agree qualitatively with those measured by Durrett et al.,[10] but velocity magnitudes here were approximately half the values reported in that study. The source of this discrepancy is not obvious, but the present results are internally consistent and exhibit no anomalies. The predicted mean radial velocities agree qualitatively with the measured values and are within the uncertainty estimate over most of the flow. Differences between the predicted and measured values are largest in the recirculation zone.

Figures 5 and 6 show profiles of the measured and modeled axial and radial turbulent normal stresses. Peak values of axial normalized turbulent intensity (i.e., the square root of the turbulent normal stress) occur in the shear layer and reach values of 25%. This is in good agreement with earlier studies performed by Gould et al.[9] and Stevenson et al.[6] The peak value of radial normalized turbulence intensity was found to be approximately 15%. This agrees closely with the findings of Durrett et al.,[10] who found peak radial normalized intensities of 17%. It is interesting to note that the peak radial normalized turbulence intensity is approximately two-thirds the value of the peak axial normalized turbulence intensity. This ratio is also characteristic of free jet flows as shown by Wygnanski and Fiedler.[21]

Calculated values of normal stresses were determined from Eqs. (2) and (3) and are represented by the dashed lines in Figs. 5 and 6. The calculated axial and radial normal stresses are

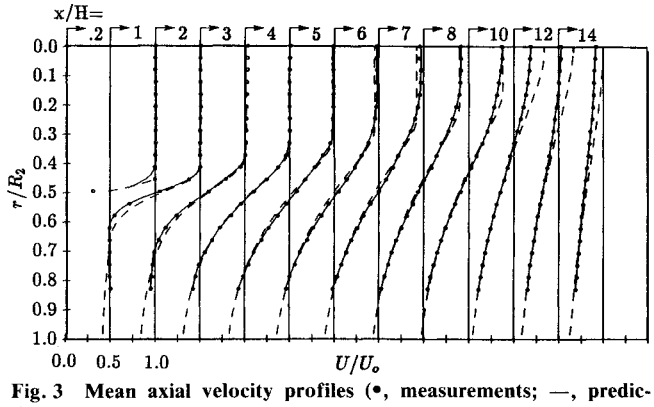

Fig. 3 Mean axial velocity profiles (•, measurements; —, prediction).

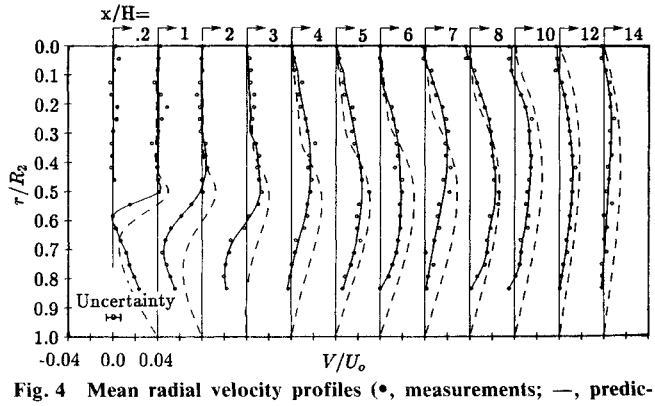

Fig. 4 Mean radial velocity profiles (•, measurements; —, prediction).

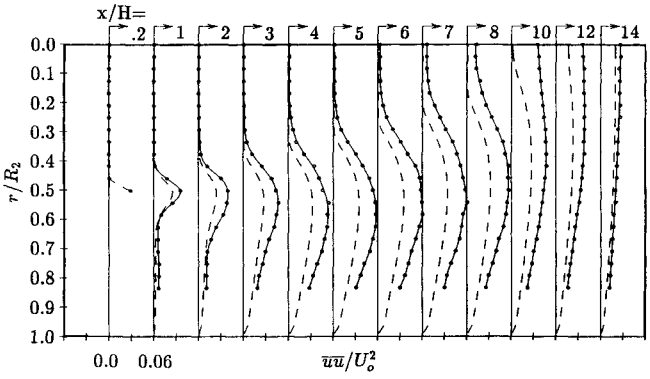

Fig. 5 Normalized axial turbulent normal stress profiles (•, measurements; —, prediction).

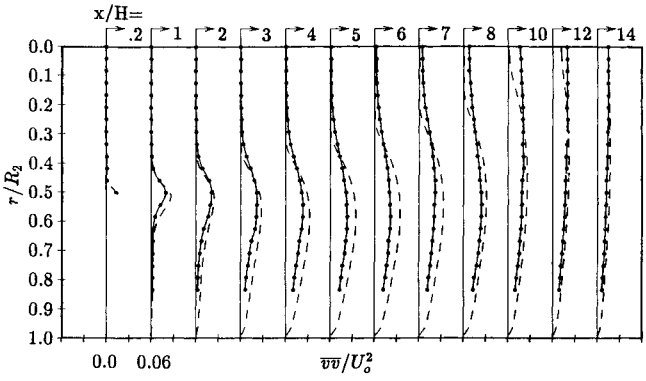

Fig. 6 Normalized radial turbulent normal stress profiles (•, measurements; —, prediction).

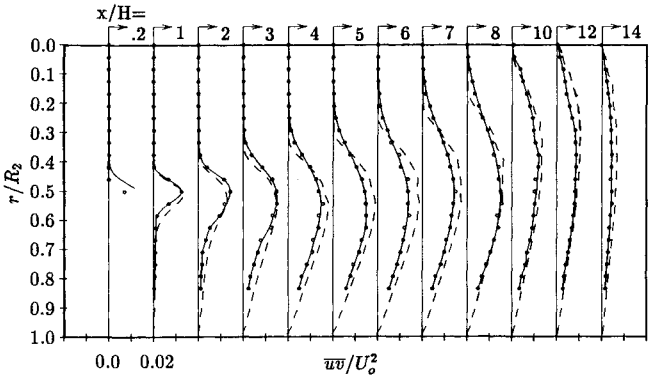

Fig. 7 Normalized shear stress profiles (•, measurements; —, prediction).

approximately equal in magnitude and profile shape, which indicates that the computed flowfield is nearly isotropic. The measured flow, however, shows considerable anisotropy in the shear layer region. This comparison shows that the calculated values are low for the axial normal stress and high for the radial normal stress. The right side of Eq. (3) consists of two parts, i.e., the contribution due to mean velocity gradients and the contribution due to the turbulent kinetic energy. This second term can be thought of as a pseudopressure and is the same numerically for all three normal stresses. In the computations done here, it accounts for 70–100% of the total normal stress values. The first term, which is due to the mean velocity gradients, is supposed to account for any anisotropy in the computed flow, but is too small to influence the calculated normal stress in this flow. A major shortcoming of the k-ϵ model and, in particular, the modified Boussinesq approximation is that it does not correctly model the anisotropy of the flow.

The values of shear stress used by the k-ϵ model are shown along with measured values in Fig. 7. Peak values of normalized Reynolds stress occur in the shear layer as expected and reach values of 0.015. This result agrees well with the results

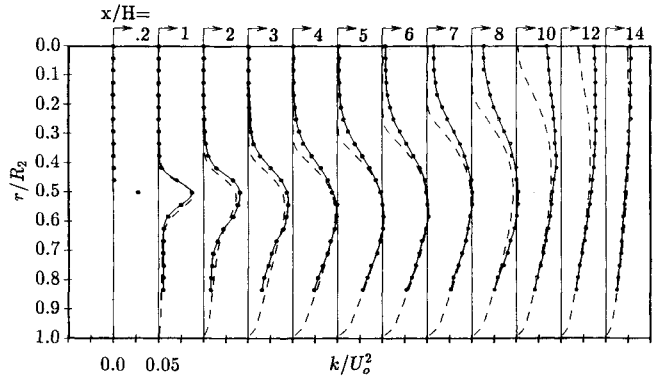

Fig. 8 Normalized turbulent kinetic energy profiles (•, measurements; —, prediction).

obtained from a study by Durrett et al.,[10] where a rotatable one-component LDV system was used along with Logan's method[22] to calculate shear stresses from two independent measurements oriented at ± 45 deg to the flow direction. The calculated shear stress values are slightly higher than the measured values in the shear layer and in the recirculation zone. Overall, the agreement is quite good. Recalling that $\overline{uv} \approx -\mu_t(\partial U/\partial r)/\rho$ in this flowfield ($\partial V/\partial x$ is small) and noting that the gradient of the measured mean axial velocities (Fig. 3) are almost identical to the predicted values (see $x/H = 3$ profile), suggests that μ_t may be too large. Equation (2) shows that incorrect values for k and/or ϵ cause μ_t to be incorrect.

Figure 8 shows the normalized turbulent kinetic energy profiles. The measured values presented here assume that the unmeasured tangential normal stress $\overline{ww}$ is equal to the measured radial normal stress $\overline{vv}$. Most researchers represent the unknown normal stress as the arithmetic mean of the two measured normal stresses [i.e., $\overline{ww} = 0.5(\overline{uu} + \overline{vv})$]. A study by Azad et al.[23] has shown that $\overline{ww} = 0.4(\overline{uu} + \overline{vv})$ for a turbulent boundary layer and fully developed pipe flow. They also found that $\overline{ww} = 0.33(\overline{uu} + \overline{vv})$ for diffuser flow. This latter relation is satisfied when $\overline{ww}$ is set equal to $\overline{vv}$ and when $2\overline{vv} = \overline{uu}$, as is the case over much of the flowfield here (see Figs. 5 and 6). In addition, free-jet experiments[20] have shown that $\overline{ww} = \overline{vv}$, and it appears to be a reasonable assumption here for measurements far from the wall ($r/R < 0.9$). The agreement between the computed and measured values of turbulent kinetic energy is quite good except that the calculated values do not diffuse radially from the shear layer, where turbulence is produced, toward the centerline at the proper rate.

One must remember that the k-ϵ model does not directly predict turbulent stresses; it solves two additional conservation equations, one for turbulent kinetic energy and one for turbulent dissipation rate, in order to define an eddy viscosity. Knowing the eddy viscosity allows one to estimate the unknown turbulent stresses in each of the conservation of momentum equations and therefore close the problem. The purpose of this analysis was to compare the modeled turbulent stresses used by the k-ϵ model with experimentally measured values. The insight gained by doing this may give rise to new turbulence models or to improvements of existing models.

Turbulent Triple Products

The turbulent triple products that are determined from the measurements made in this study are $\overline{uuu}$, $\overline{uuv}$, $\overline{uvv}$, and $\overline{vvv}$. The normalized values are shown in Figs. 9–12. The triple products are antisymmetric about the centerline of the shear layer, peaking to either side of the shear layer and approaching zero at the edges. This behavior is characteristic of free shear layers in early stages of separation. Negative values of $\overline{uuu}$, as seen on the centerline side of the shear layer, indicate as expected that the axial velocity probability distributions

are skewed with a larger number of high velocity samples. Very little data exists that can be compared to the present triple product data. Driver and Seegmiller[4] present limited triple product data (i.e., the sum of $\overline{uuv}$ and $\overline{vvv}$) in the flowfield downstream of a 2-D backward-facing step. The other two triple products, although interesting, probably were not presented because the radial gradient of $(\overline{uuv} + \overline{vvv})$ dominates the turbulent diffusion process in sudden expansion flows. The triple product profiles from the present study, and Driver and Seegmiller's study exhibit similar shapes but differ in peak magnitudes. The peak normalized values of $(\overline{uuv} + \overline{vvv})$ were found to be approximately 5 times greater in this study than those reported by Driver and Seegmiller. By comparison, the normalized peak values of Reynolds stress in this study were found to be 1.5 times greater than those reported by Driver and Seegmiller for the 2-D backward facing step flow. One possible reason for the large difference in measured magnitude may be the large disparity in expansion ratio used in the two studies. Driver and Seegmiller used an expansion ratio of 1.125:1; while an expansion ratio of 4:1 was used for the present study. Driver and Seegmiller also reported that $(\overline{uuu} + \overline{uvv})$ exhibited similar behavior to $(\overline{uuv} + \overline{vvv})$ but was opposite in sign. Profiles of the four measured triple products in this study exhibited the same general behavior but did not change sign. The sign change is a result of the chosen coordinate system. Driver and Seegmiller measured a positive y direction away from the wall, while the positive r direction was measured from the centerline (toward the wall) in the present study. The relatively large negative value of $\overline{uuu}$ on the centerline of the sudden expansion at $x/H = 10$ (Fig. 9) indicates that relatively more high velocity parcels of fluid from the decaying central core region are passing through this region. This behavior, unidentified until now, may be a fundamental characteristic of axisymmetric sudden expansion flow. It may indicate the passage of large eddy structures or that the central core region is oscillating at some resonant frequency. In defense of this data, the value of $\overline{uu}$ at this location was found to be reasonable, which strongly suggests that $\overline{uuu}$ is also reasonable.

Turbulent Kinetic Energy Balance

In the k-ϵ turbulence model, k is the turbulent kinetic energy (TKE) defined by Eq. (1), and ϵ is the rate of turbulent dissipation. The set of governing equations for an incompressible, axisymmetric turbulent flow are a set of five coupled, nonlinear, partial-differential equations that are solved numerically with the appropriate boundary conditions for the dependent variables U, V, P, k, and ϵ. Three of the governing equations are the time-averaged continuity equation and the axial and radial momentum equations with the viscosity set equal to the effective viscosity; that is

$$\mu_{\text{eff}} = \mu_t + \mu_{lam} \tag{4}$$

where μ_t is related to k and ϵ by Eq. (2). In addition, there is a modeled transport equation for turbulent dissipation rate[24] and a modeled transport equation for turbulent kinetic energy. The modeled TKE equation for steady, incompressible, axisymmetric flow is given by

$$\frac{1}{r}\frac{\partial (r\rho Vk)}{\partial r} + \frac{\partial (\rho Uk)}{\partial x} - \frac{1}{r}\frac{\partial}{\partial r}\left[\mu_{\text{eff}}\, r \frac{\partial k}{\partial r}\right] - \frac{\partial}{\partial x}\left[\mu_{eff}\frac{\partial k}{\partial x}\right]$$

$$- \mu_t\left[2\left[\frac{\partial U}{\partial x}\right]^2 + 2\left[\frac{\partial V}{\partial r}\right]^2 + \left[\frac{\partial V}{\partial x} + \frac{\partial U}{\partial r}\right]^2\right] + \rho\epsilon = 0 \tag{5}$$

In Eq. (5) the terms represent 1) radial and axial convection of TKE, 2) radial and axial diffusion of TKE, 3) production of TKE, and 4) dissipation of TKE. The complete transport

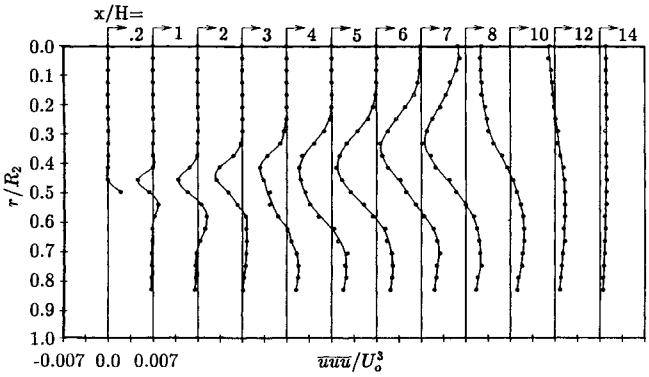

Fig. 9 Normalized $\overline{uuu}$ turbulent triple product profiles (•, measurements).

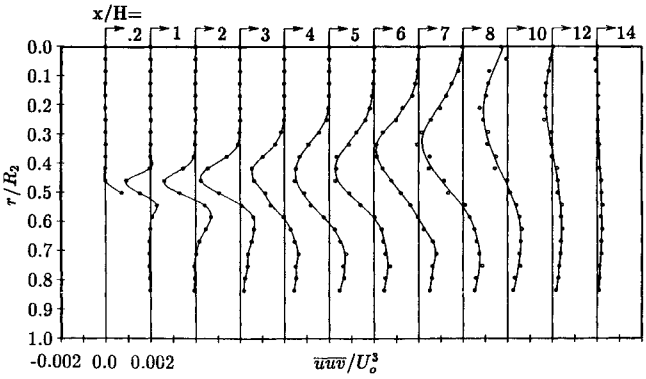

Fig. 10 Normalized $\overline{uuv}$ turbulent triple product profiles (•, measurements).

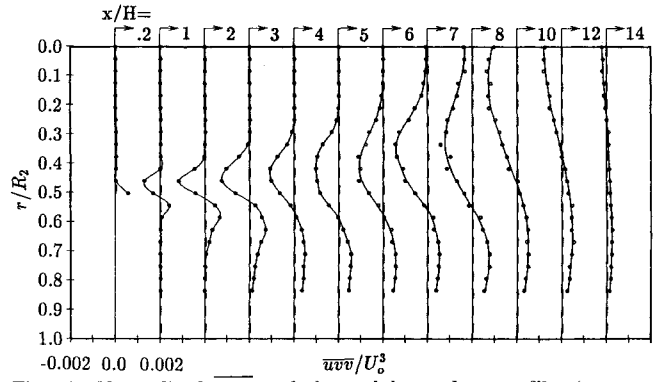

Fig. 11 Normalized $\overline{uvv}$ turbulent triple product profiles (•, measurements).

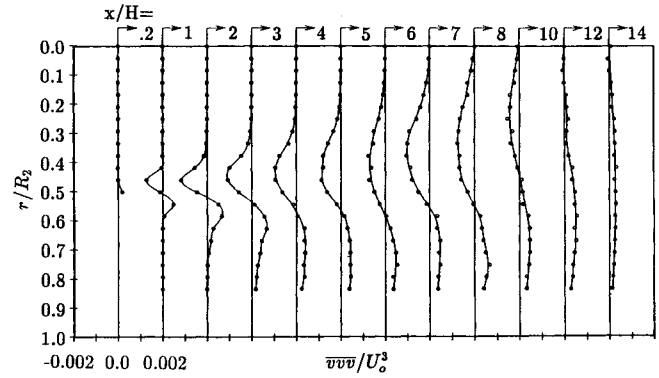

Fig. 12 Normalized $\overline{vvv}$ turbulent triple product profiles (•, measurements).

equation for turbulent kinetic energy in a steady incompressible, axisymmetric flow is given by

$$\frac{1}{r}\frac{\partial (r\rho Vk)}{\partial r} + \frac{\partial (\rho Uk)}{\partial x}$$

$$-\frac{1}{r}\frac{\partial}{\partial r}\left[\mu r\frac{\partial k}{\partial r} - \rho r\frac{\overline{vvv}}{2} - \rho r\frac{\overline{vww}}{2} - \rho r\frac{\overline{uuv}}{2} - r\overline{vp}\right]$$

$$-\frac{\partial}{\partial x}\left[\mu\frac{\partial k}{\partial x} - \rho\frac{\overline{uuu}}{2} - \rho\frac{\overline{uvv}}{2} - \rho\frac{\overline{uww}}{2} - \overline{up}\right]$$

$$+\left[\mu\frac{\overline{vv}}{r^2} + \mu\frac{\overline{ww}}{r^2}\right]$$

$$+\left[\rho\overline{vv}\frac{\partial V}{\partial r} + \rho\overline{uv}\frac{\partial U}{\partial r} + \rho\overline{uv}\frac{\partial V}{\partial x} + \rho\overline{uu}\frac{\partial U}{\partial x} + \rho\overline{ww}\frac{V}{r}\right]$$

$$+\mu\left[\overline{\left[\frac{\partial v}{\partial r}\right]^2} + \overline{\left[\frac{\partial w}{\partial r}\right]^2} + \overline{\left[\frac{\partial u}{\partial r}\right]^2} + \overline{\left[\frac{\partial v}{\partial x}\right]^2} + \overline{\left[\frac{\partial w}{\partial x}\right]^2}\right.$$

$$\left.+\overline{\left[\frac{\partial u}{\partial x}\right]^2}\right] = 0 \qquad (6)$$

where the fluctuating axial, radial, and tangential velocities are denoted by u, v, and w, respectively. Equation (6) is composed of the following terms: 1) radial and axial convection, 2a) radial diffusion, 2b) axial diffusion, 2c) additional diffusion due to cylindrical coordinates, 3) production, and 4) viscous dissipation. The exact TKE equation has many additional unknowns, including gradients of triple products, pressure diffusion terms, and viscous dissipation terms. In order to simplify this exact TKE equation to the form given by Eq. (5), the unknown terms are either modeled as a function of some known quantity or are completely ignored. In an effort to validate the transport equation for turbulent kinetic energy, an energy balance was performed as part of this study.

Figures 13–16 compare the calculated values of convection, production, diffusion, and dissipation of TKE in Eq. (5) with the measured values in Eq. (6). The calculated values in Eq. (5) were determined from the converged numerical solution from the TEACH code. Numerical central-difference operators were used to evaluate the first and second derivatives. The exact TKE equation, Eq. (6), contains some terms that were not measured. The following assumptions were made: $\overline{ww} = \overline{vv}$, $\overline{vww} = \overline{vvv}$, and $\overline{uww} = \overline{uvv}$. In addition, the pressure-diffusion terms $\overline{up}$ and $\overline{vp}$ were assumed to be negligible, which is a reasonable assumption at locations away from the wall. The experimental data were smoothed before the derivatives were evaluated using a least-squares cubic-spline smoothing package. The "measured" dissipation was inferred by balancing Eq. (6), whereas the modeled dissipation is a direct output of the TEACH code.

A number of conclusions can be drawn from these results. First, the predicted production of turbulent kinetic energy differed from the measured values in the same manner as the predicted and measured Reynolds stress profiles (see Fig. 7). This is because the total production of turbulent kinetic energy is dominated by the $\overline{uv}\partial U/\partial r$ term in this flowfield. The terms containing the turbulent normal stresses contribute very little to the production of turbulent kinetic energy. As a result, the

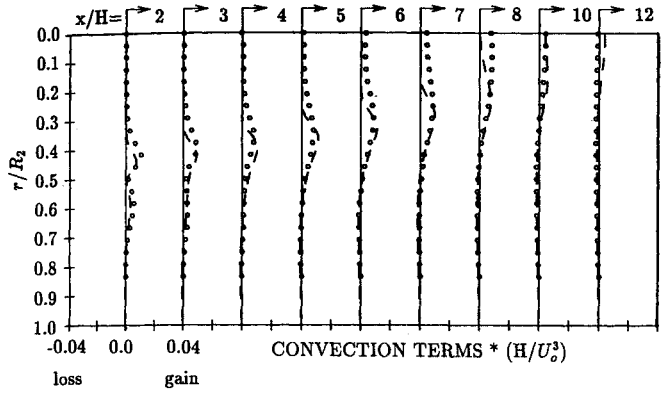

Fig. 13 Normalized convection of turbulent kinetic energy (•, measurements; —, prediction).

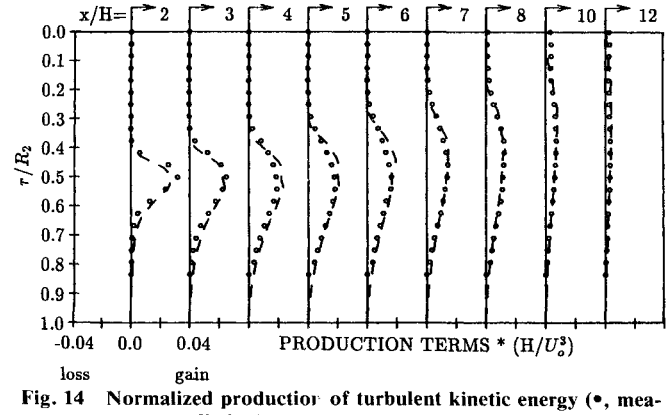

Fig. 14 Normalized production of turbulent kinetic energy (•, measurements; —, prediction).

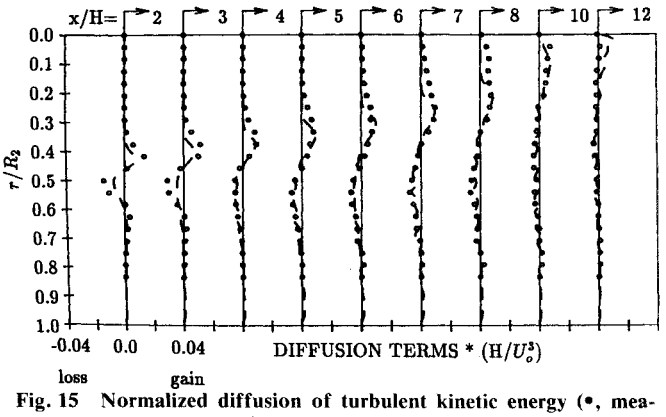

Fig. 15 Normalized diffusion of turbulent kinetic energy (•, measurements; —, prediction).

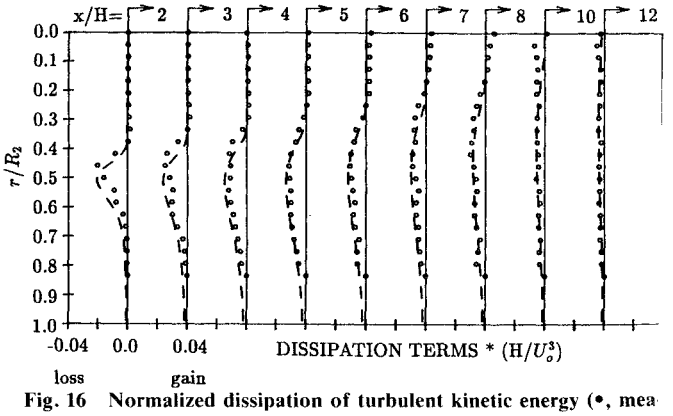

Fig. 16 Normalized dissipation of turbulent kinetic energy (•, measurements; —, prediction).

predicted mean flowfield is in good agreement with the measured flowfield in spite of the poor turbulent normal stress modeling.

The predicted convection of turbulent kinetic energy was found to be lower than the measured convection in the central region of the flow downstream of $x/H = 6$. Convection of TKE is represented exactly in the modeled equation; therefore, this result is due primarily to the poorly modeled diffusion terms. The radial gradients of $\overline{uuv}$ and $\overline{vvv}$ give rise to high values of measured turbulent diffusion in this region. Apparently, the transport coefficient μ_t used in the modeled diffusion terms does a poor job of modeling the actual diffusion in this region of the flow. Turbulent kinetic energy is produced in the shear layer but is not diffused radially toward the centerline in the predicted flow. If the radial diffusion of turbulent kinetic energy from the shear layer region to the centerline of the flow in underpredicted, then the values of turbulent kinetic energy k near the centerline will be low, as shown in Fig. 8. The profiles of U, V, and k indicate that bulk convection of turbulent kinetic energy proceeds in a direction away from the central core region.

Summary and Conclusions

A two-component LDV was used to measure accurately U, V, $\overline{uu}$, $\overline{vv}$, $\overline{uv}$, $\overline{uuu}$, $\overline{uuv}$, $\overline{uvv}$, and $\overline{vvv}$ in the flowfield downstream of an axisymmetric sudden expansion. The triple product data are unique in that practically no other triple product data are available. The measured values of U, V, $\overline{uu}$, $\overline{vv}$, and $\overline{uv}$, and turbulent kinetic energy k are compared to the computed values based on the k-ϵ turbulence model. Comparison of measured and calculated values of U are remarkably good except for a region where the turbulent mixing layer reaches the axis (i.e., the central core region downstream of $x/H = 6$). Comparison of V profiles is not nearly as good. Agreement between the measured and calculated turbulent shear stress $\overline{uv}$ and k is quite good except that the radial diffusion of TKE from the shear layer to the centerline is underpredicted by the k-ϵ model. Comparison of the turbulent normal stresses expose one of the major failings of the modified Boussinesq approximation, namely that it does not properly account for anisotropy of the flow. The axial turbulent normal stresses are considerably underpredicted, whereas the radial values are overpredicted. In lieu of using the full transport equations for Reynolds stresses[25] or the simplified algebraic stress model,[26] a modification to the eddy viscosity model aimed at correcting this error may be a fruitful area of study. Turbulent triple products were measured and found to contribute significantly to the transport of turbulent kinetic energy. A turbulent kinetic energy balance identified the various areas of the flow where different turbulent transport mechanisms dominate. Finally, the k-ϵ model appears to do a very respectable job in modeling this particular flowfield.

Acknowledgment

This investigation was supported by NASA Lewis Research Center under Grant NAG3-502.

References

[1]Durrett, R. P., Gould, R. D., Stevenson, W. H., and Thompson, H. D., "A Correction Lens for Laser Doppler Velocimeter Measurements in a Cylindrical Tube," *AIAA Journal,* Vol. 23, Sept. 1985, pp. 1387–1391.

[2]Eaton, J. K. and Johnston, J. P., "An Evaluation of Data for Backward Facing Step Flow," *1980/81 Conferences on Complex Turbulent Flows,* Department of Mechanical Engineering, Stanford University, Palo Alto, CA 1980.

[3]Bremmer, R., Thompson, H. D., and Stevenson, W. H., "An Experimental and Numerical Comparison of Turbulent Flow Over a Step," Air Force Wright Aeronautical Laboratories, AFWAL-TR-80-22105, 1980.

[4]Driver, D. M. and Seegmiller, H. L., "Features of a Reattaching Turbulent Shear Layer in Divergent Channel Flow," *AIAA Journal,* Vol. 23, Feb. 1985, pp. 163–171.

[5]Pitz, R. W. and Daily, J. W., "Combustion in a Turbulent Mixing Layer Formed at a Rearward-Facing Step," *AIAA Journal,* Vol. 21, Nov. 1983, pp. 1565–1570.

[6]Stevenson, W. H., Thompson, H. D., and Luchik, T. S., "Laser Velocimeter Measurements and Analysis in Turbulent Flows with Combustion," Part I, Air Force Wright Aeronautical Laboratories, AFWAL-TR-82-2076, Part I, Dayton, OH, 1982.

[7]Freeman, A. R., "Laser Anemometer Measurements in the Recirculating Region Downstream of a Sudden Pipe Expansion" *Proceedings of the LDA-Symposium,* Denmark, 1975.

[8]Moon, L. F. and Rudinger, G., "Velocity Distribution in an Abruptly Expanding Circular Duct," *ASME Journal of Fluids Engineering,* Vol. 99, 1977, pp. 226–230.

[9]Gould, R. D., Stevenson, W. H., and Thompson, H. D., "Laser Velocimeter Measurements in a Dump Combustor" ASME Paper 83-HT-47, 1983.

[10]Durrett, R. P., Stevenson, W. H., and Thompson, H. D., "Radial and Axial Turbulent Flow Measurements with an LDV in an Axisymmetric Sudden Expansion Air Flow," *ASME Journal of Fluids Engineering,* Vol. 110, 1988, pp. 367–372.

[11]Stevenson, W. H., Thompson, H. D., and Roesler, T. C., "Direct Measurement of Laser Velocimeter Bias Errors in a Turbulent Flow," *AIAA Journal,* Vol. 20, 1982, pp. 1720–1723.

[12]Johnson, D. A., Modarress, D., and Owen, F. K., "An Experimental Verification of Laser-Velocimeter Sampling Bias Correction," *Proceedings of the Symposium on Engineering Applications of Laser Velocimetry,* American Society of Mechanical Engineers, New York, Nov. 1982, pp. 153–162.

[13]Gould, R. D., Stevenson, W. H., and Thompson, H. D., "A Parametric Study of Statistical Velocity Bias," *AIAA Journal,* Vol. 27, No. 8, 1989, pp. 1140–1142.

[14]Yanta, W. J. and Smith, R. A., "Measurements of Turbulence-Transport Properties with a Laser Doppler Velocimeter," AIAA Paper 73-169, 1973.

[15]Pun, W. M. and Spalding, D. B., "A General Computer Program for Two-Dimensional Elliptic Flows," Mechanical Engineering Dept., Imperial College, London, England, 1976.

[16]Chiappetta, L. M., "User's Manual for a TEACH Computer Program for the Analysis of Turbulent, Swirling Reacting Flow in a Research Combustor," NASA Rept. HTS/76/2, R83-915540-27, 1983.

[17]Magnussen, B. F. and Hjertager, B. H., "On Mathematical Modeling of Turbulent Combustion with Special Emphasis on Soot Formation and Combustion," *Proceedings of the 16th Symposium (International) on Combustion,* The Combustion Institute, 1978, pp. 719–729.

[18]Raithby, G. D., "Skew Upwind Differencing for Problems Involving Fluid Flow," *Computational Methods in Applied Mechanics and Engineering,* Vol. 9, 1976, pp. 153–166.

[19]Hinze, J. O., *Turbulence,* 2nd ed., McGraw-Hill, New York, 1975.

[20]Stevenson, W. H., Thompson, H. D., and Craig, R. R., "Laser Velocimeter Measurements in Highly Turbulent Recirculating Flows," *Proceedings of the Symposium on Engineering Applicatiaons of Laser Velocimetry,* American Society of Mechanical Engineers, New York, 1982.

[21]Wygnanski, I. and Fiedler, "Some Measurements in the Self-Preserving Jet," *Journal of Fluid Mechanics,* Vol. 38, 1969, p. 577.

[22]Logan, S. E., "A Laser Velocimeter for Reynolds Stresses and Other Turbulence Parameters," *AIAA Journal,* Vol. 19, 1972, pp. 933–935.

[23]Azad, R. S., Kassab, S. Z., and Dang, T. H., "Experimental Evaluation of Approximations for $\overline{w^2}$ and $\overline{vw^2}$," *AIAA Journal,* Vol. 25, 1987, pp. 171–173.

[24]Harlow, F. H. and Nakayama, P. I., "Transport of Turbulence Energy Decay Rate," Los Alamos Science Laboratory, University of California, Rept. LA-3854, 1968.

[25]Launder, B. E., Reece, G. J., and Rodi, W., "Progress in the Development of a Reynolds-Stress Turbulence Closure," *Journal of Fluid Mechanics,* Vol. 68, 1975, pp. 537–566.

[26]Rodi, W., "A New Algebraic Relation for Calculating the Reynolds Stresses," *ZAMM*, Vol. 66, 1976, pp. T219–T221.